SSC17-P2-03

Space Webs as Infrastructure for Crawling Sensors on Low Gravity Bodies

Juliana Cherston, Joseph A. Paradiso
Responsive Environments Group, MIT Media Lab
75 Amherst Street, Cambridge MA 20139; 917-921-9864
Cherston@mit.edu

ABSTRACT

This paper presents a mission concept in which a rope or a net is used to grapple onto a low-gravity body of interest. The net doubles as infrastructure for a network of tiny crawlers that move across the net's surface primarily for applications in in-situ distributed sensing. As an initial application area, we consider deploying a network of distributed spectrometers across the surface of an asteroid for high spatial resolution material characterization. We present a first prototype for a rope crawling mechanism as well as a study of a new-to-market chip-sized spectroscope as a candidate sensing payload for the crawlers. Some evidence is found for the sensor's ability to discriminate between high-iron and low-iron meteorite samples.

INTRODUCTION

It is notoriously difficult to build rovers that can land and move on low-gravity bodies. In spite of this difficulty, any application in distributed in-situ sensing of a low-gravity body will require that many such rovers land successfully.

We imagine using a many-kilometer-long net (or rope) to grapple onto a small body of interest. The net doubles as infrastructure for a network of possibly hundreds to thousands of tiny crawling robots that move across the body's surface.

Numerous applications can be imagined for a distributed sensor network deployed onto a body via net. For instance, high resolution seismic data can be acquired using a network of vibration sensors and an impactor. If an internal region-of-interest is identified, crawlers can congregate in the region-of-interest for even higher resolution seismography.

Similarly, the net can enable distributed tomography experiments using either an x-ray/alpha source from an orbiting satellite or using a natural cosmic ray source.

More broadly, the low-gravity object can serve as a rigid body onto which a large, distributed aperture imager or phased array antenna is deployed. So long as the low-gravity body faces a region-of-interest in the sky, the passive rigidity provided by the body removes the need for fine stabilization of the net that would be required for an equivalent mission conducted in orbit.

In the nearer term, it may also be worthwhile to explore applications involving throwing a net of crawlers at a defunct satellite for repair scenarios or for repurposing modules such as antenna.

In the current work, we choose to focus on distributed reflectance spectroscopy for high spatial resolution prospecting of an asteroid's surface. We may also study other listed application areas in the future. The network of high spatial resolution spectroscopes work in tandem with a high spectral resolution orbital spectrometer that guides the crawlers to regions of interest. The resulting data can contribute useful knowledge about the material composition of small bodies e.g. for asteroid mining missions. If the crawlers are equipped with actuators (magnetic rakes, drills, etc.), they can also be tasked with stockpiling material.

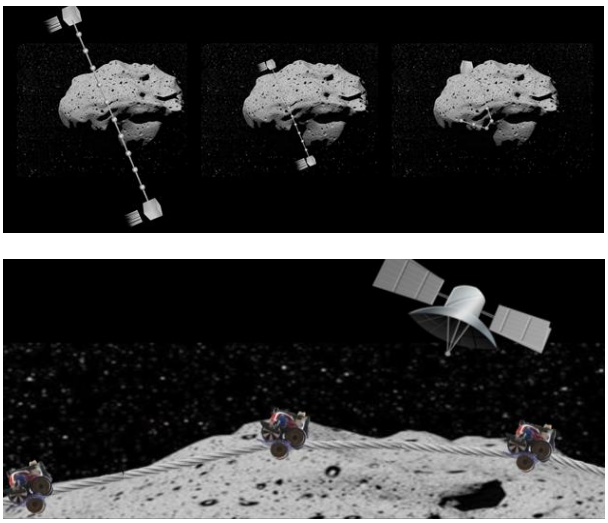

Figure 1: Two Mission Concept Drawings

This paper serves as an initial inquiry into the overall mission concept. A new-to-market, $8 multispectral imager is evaluated for its usefulness as a sensing payload. Preliminary evidence is presented for effective discrimination between high and low iron meteorite samples using this chip. Finally, an initial prototype for a rope crawling mechanism is presented.

BACKGROUND

The concept of distributed sensor deployment via net across a body lies at the intersection of a number of emerging research areas in space exploration technology including the miniaturization of satellites down to as small as femtosatellite scale, the development of satellite swarms to cooperatively accomplish space-based missions, a growing interest in developing novel approaches for landing on low-gravity bodies, and most centrally, the productive use of nets in microgravity conditions.

Regarding the prior study of nets in space, two applications are most commonly addressed: the use of nets for deploying largescale infrastructure in orbit and the use of nets for orbital debris capture. The proposed mission is a novel concept that draws from each of these applications areas: rather than catch debris, we catch bodies of scientific interest; rather than use crawlers for remote sensing, we deploy them directly across the body for in-situ sensing.

Space Webs For Distributed Sensing

Space nets (traditionally called 'Space-Webs') have been recognized as an effective means for deploying distributed aperture interferometers, phased array antenna, and solar arrays in orbit, among other potential application areas. Nets can be packaged in low-volume containers during launch and deployed into certain well-studied stable configurations. Gärdsback has studied control algorithms for the net deployment phase in depth, favoring a star-shaped net release pattern [1]. Proposals for stabilizing nets in orbit most commonly involve a 2D rotating net that is modeled using the Melnikov-Koshelev control law (relating control torque to angular velocity), though some models for stable 3D Earth-facing structures have been developed as well [2]. Finally, Kaya et al. were the first to propose the use of a spider-like crawling robot on a space net [3].

Unfortunately, both attempts in recent history at testing net dynamics in microgravity have encountered technical difficulties: in 2006, the Furoshiki mission (motivated by the work of Kaya et al.) deployed a space web with three crawlers off of a sounding rocket, but a misaligned radial thruster resulted in chaotic deployment [4, 5]. In 2012, the Suaineadh experiment deployed a spinning space web off a sounding rocket but the wireless data transmission scheme was interrupted during web deployment [6]. That said, in 2010, Japan successfully launched the 14 meter IKAROS solar sail which serves as an initial proof-of-concept for deployment of thin membranes in orbit [7].

An application of great interest for nets in orbit involves using the net to beam power to ground. In pursuit of this goal, the ESA conducted a study on the deployment of a 10km long space-web in geostationary orbit that would benefit from unobstructed view of the sun for power harvesting; solar collectors are deposited along the net using robotic crawlers and power is beamed to earth via microwaves [8]. This proposal is yet to be directly tested.

Space Webs for Orbital Debris Capture

An extensive study of the use of space webs for orbital debris capture is conducted by Yang et al [9]. Various mission concepts have been proposed for removing orbital debris using nets. These include (1) a tether-net system to tug orbital debris into designated graveyard orbits [10] (2) a free net with thrust at each corner [11] (3) a magnetic net that comes into close proximity to the target [12], among other possibilities. We imagine that net dynamics models developed for orbital debris capture can ultimately be repurposed for landing distributed sensor arrays on small bodies.

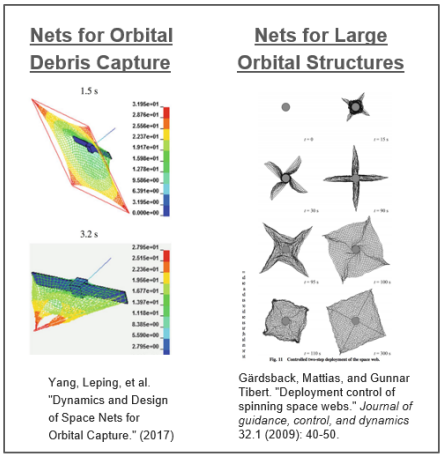

Figure 2: Excerpts from prior art in net dynamics

MISSION OVERVIEW

High Level Summary

The high-level mission concept is as follows:

1. Mothership launches carrying high resolution spectral imager, optimally folded Kevlar net, and swarm of crawlers

2. Mothership approaches low-gravity body of interest and shoots net at body via net gun

3. Net adheres to surface of body

4. High spectral resolution spectrometer aboard mothership scans body for regions of interest

5. Crawlers already onboard the net are guided by mothership to regions of interest for high spatial resolution imaging; algorithms for swarm control regulate the motion of each crawler; the crawlers are redundant - if a subset were to malfunction, the mission can still succeed.

6. [If part of larger asteroid mining mission] Crawlers can be instructed to image, drill, and pick up samples of interest and carry them to a processing zone

In order for the aforementioned steps to be carried out, a number of sub-studies are required in order to develop and validate technology central to the mission. These sub studies are summarized in Figure 3.

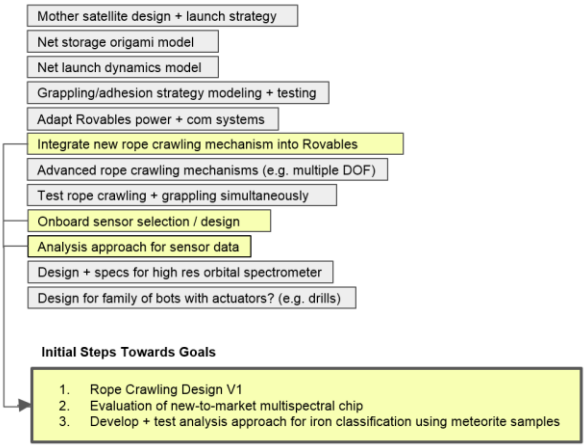

Figure 3: Mission sub studies required which initial steps highlighted

Adherence of Net to Body

A study on the adherence of a net to a body of interest will ultimately be of central importance for proving out the proposed mission. Single point-of-contact anchors used in prior low-gravity lander missions are susceptible to failure. For example, in 2014 the Philae comet lander anchoring harpoon did not fire, adding substantial risk to the mission's success.

In contrast, a rope or a net provides several contact points for attaching to the body and therefore has increased failure tolerance. There are a variety of adhesion methods worth considering. To provide a few examples: (1) the net may extrude a fast-setting adhesive upon contact, (2) if landing on an icy surface, precisely controlled contact melting can be used to freeze the net in place (3) a bi-stable mechanism can be considered in which segments of the rope snap onto the body upon contact.

Net as Infrastructure

Most grappling technologies are by nature designed to fix the lander in one position on the low-gravity body and do not allow for motion, whereas a net provides the possibility for crawlers to move across the body's surface. Further, if a region of the net is dedicated to solar power harvesting, it may be possible to enable wired transmission of harvested power to the crawling bots. Wired communication between the bots may also prove an advantageous benefit of the net and will be considered.

Initial Steps

To justify the premise of the mission, it is first necessary to define a sensing payload that motivates the mission; in order to demonstrate that the sensing payload will be effective, a precision rope crawling mechanism is needed. For these reasons, initial work has focused on studying candidate sensing payloads as well as building a crawling mechanism prototype. Note that for the purpose of developing a fully functional crawler, our team's Rovables project – focused on designing robots to crawl on clothing – may ultimately be adapted to suit the requirements for a space-based crawler [13].

To commence the design process, a set of target metrics have been specified for key components of the project. These are listed in Table 1 and Table 2.

Table 1: Tethered Microrobot Specifications

Size	Nominally aiming for 3'' x 3'' x 3''
Weight	Nominally aiming for 150g
Power	Nominally aiming to sustain 30 min of motion or 8 hours without motion per charge cycle*****
Cost	< $75 / crawler

* matches Rovables target

Table 2: Targets Metrics For Largescale System

Net Size	Up to 10's of km
Orbital Spectrometer Ground Resolution	1-2 m
Crawling Spectrometer Spatial resolution	< 10 cm
Total # of Crawlers	100's – 1000's

AS7263 MULTISPECTRAL CHIP

Selection of Spectrometer

The AS7263 is a new-to-market (Jan, 2017) chip-sized multispectral sensor with sensitivity in six bands in the VIS-NIR spectral range, each 20nm full width half max [14]. The spectral sensitivity of the chip is pictured in Figure 5. The chip is composed of 6 nano-optic deposited interference filters placed on standard CMOS silicon and an onboard 0.75mm pinhole aperture. It has a footprint of only 4mm^2 and a cost of only $8. It is the only chip of its kind on the market at the quoted size and price point. A survey of small spectrometers under $1000 in cost was conducted which lead to the selection of the AS7263 for evaluation. This survey is presented in Table 3.

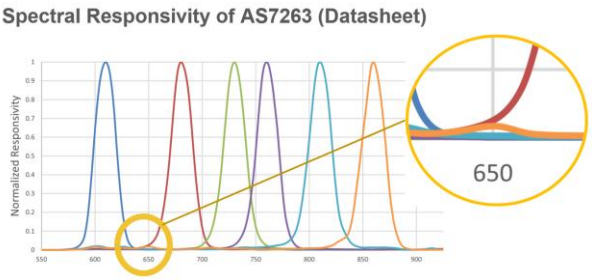

Figure 5: Closeup of the spectral responsivity of the AS7263 including a zoomed view at 650nm

The AS7263 is found to be one to two order-of-magnitude cheaper than all other commercial-off-the-shelf spectrometers. Its tiny form factor and sensitivity in the NIR range make it a particularly appealing candidate sensor, especially in the case where hundreds to thousands of sensor nodes are needed for scanning a low-gravity body. There may be a wealth of applications for a chip of this sort in the context of small satellite development.

During calibration tests, responsivity to a diffuse 650nm laser is found to be within error margins. However, responsivity to a calibrated halogen light source is found to be erroneous and variable, possibly due to extreme sensitivity of the sensor to incidence angle of light. Additional optics tests will soon be conducted. If necessary the Nano Lambda sensor can be evaluated as an alternative COTS component for the proposed mission. Despite an order-of-magnitude higher price point than the AS7263 and a larger form factor, it provides spectral sensing at significantly higher resolution. (see Table 3 for specifications).

Table 3: Summary of COTS Micro-Spectrometers

Sensor	Spectral Range	Size (mm)	Price**
Texas Instruments NIR Spectrometer	1824 bands in 900-1700 nm range	33 × 29 ×10	$999
Ocean Optics Spark-DET-VIS	~80 bands in 380-700 nm range	18 x 10 x 0.3	$309
Hamamatsu C12880MA Micro Spectrometer	~288 bands in 340-850 nm range	20 x 13 x 10	$245
PixelSensor	8 bands in 425-850nm range	46 x 21 x 5	$195
Nano Lambda NSP32	4 products: ~20-40 bands in (390-760nm, 600-1000nm, 850-1050nm, 400-1000nm)	18 x 7 x 6	$148
AS7263	**6 bands from 610 - 860nm**	**5 x 5 x 2.5**	**$8**

**Prices quoted for sensors, not for dev kits

IRON CLASSIFICATION IN METEORITES USING THE AS7263 SENSOR

Background

As an initial test, measurements of meteorite samples were taken using the AS7263 in order to study whether the samples can be classified in terms of iron content. There were various motivations for targeting iron classification as an initial classification study. Broadly, iron is recognized as a viable and plentiful building material for space-based construction. Asteroid regolith is also thought to contain compounds rich in iron, thereby opening the possibility for the crawlers to collectively build up a stockpile of iron-rich construction material. Finally, even if prospecting missions ultimately focus on collecting oxygen and hydrogen rich compounds for fuel and water production in space, it will be important to accurately characterize the iron-rich background.

More specifically, meteorites are already classified in terms of their iron content, thereby providing a codified means for distinguishing between sample types. Further, visible/near-infrared (400-1000nm) spectra are commonly used to constrain mineralogy of iron-bearing minerals on Mars and other remote bodies. For example, the spectral signature of 0.85um/0.6um is used for iron oxide characterization in soil, and the spectral signature of 1.55um/0.76um is used for ferrous material characterization. A decrease in reflectance towards the near-infrared is attributable to the presence of iron absorption bands such as pyroxenes and olivine (Fe^{2+}). Positive slopes from the blue to red wavelengths with maxima near 750nm are a sign of Fe^{3+} absorption. The ratio of red reflectance to blue reflectance can be used as an indicator for the relative level of oxidation of materials and/or the degree of dust coating on surfaces. For example, relatively dust-free rocks observed by in-situ multispectral imagers on Mars exhibit lower red/blue color ratios than more dust-coated surfaces [15]. Hence there is scientific basis for believing that iron content classification is possible using a spectral sensor sensitive in the visible/near-infrared range. It remains to determine whether six spectral bands can suffice for drawing conclusions about iron content.

Motivation

While work is ongoing to validate the calibration of the AS7263, evaluation of the sensor has also shown measurement repeatability for each specific setup. Therefore, in the case where a light source is mounted to the spectral sensing board and held at consistent distance and angle from an imaging sample, there may still be meaningful patterns in the spectral data. Further, the analysis approach presented in this section can later be followed even if additional calibration of the data is found to be required. One limitation worth emphasizing is that the spectra cannot currently be analyzed in terms of standard spectral signatures for iron (some of which were outlined in the prior section). These spectral signatures will be considered once the calibration of the sensor is validated.

Setup

Eight meteorite samples were obtained through the MIT Earth and Planetary Sciences department for preliminary analysis. 17 samples from unique meteorites (23 samples in total) from the Harvard Geological Museum collection were then used for the full study during a daylong visit to the collection. The samples range in iron content and were categorized based on the classes defined in Table 4, all standard metrics for classifying chondrites and iron meteorites. The few samples that were neither chondrites nor iron meteorites were classified based on how their iron content compared to the listed percentages per class.

Table 4: Iron Classification in Meteorites

Iron (IVA, IVB, etc.)

'HH'	90%+ Iron (predominantly metallic)

Chondrites

H	High Iron (25-30% Iron, 50% in metallic)
L	Low Iron (20-25% Iron, 5-10% metallic)
LL	Very Low Iron (<20% Iron, 0.3-3% metallic)

A 2.5 volt, 0.1mA halogen bulb was used as a light source. It was mounted directly to the development board and controlled via an external trigger button and via the AS7263's built-in shutter control. The I^2C protocol was used for communication with the sensor, and the chip was set to a gain of 64x (maximum) and an integration time of 280ms for all exposures. Note that during the proposed mission it will likely be possible to use sunlight as an illumination source rather than rely on a power-intensive halogen bulb.

The sensor was clamped to a shelf in a darkroom. Samples were placed on a black velvet background and moved by hand across the aperture in order to generate synthetic pixels. Two spectra were captured per location and averaged. 15 spectra per row were acquired, and between 1 and 5 rows of spectra were acquired depending on the size of the sample. In this way, a low resolution spectral image with pixel count ranging from 15 to 75 was acquired for each sample. The sensor set up and experimental procedure are shown in Figure 6.

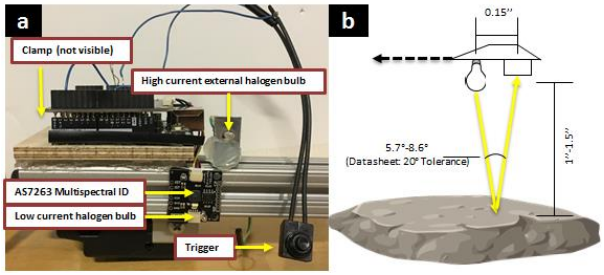

Figure 6: Meteorite Reflectance Spectroscopy Experimental Setup (left) and procedure (right)

Data Preprocessing

Each exposure contains spectral information composed of a linear combination of the sample's spectrum and the black background's spectrum as in Equation 1. Relative percentages depend on the sample size as well

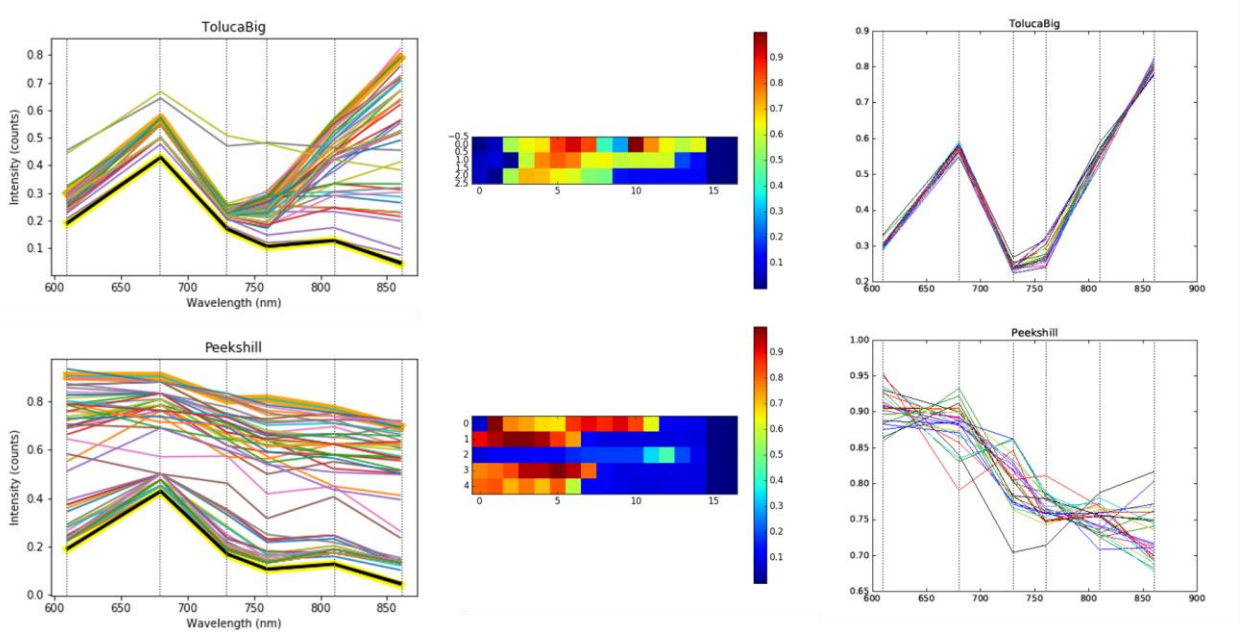

Figure 7: Multispectral data preprocessing steps shown for two distinct meteorite samples. Vertical lines indicate peak sensitivity bands of AS7263. Left: plots of all pixels taken for the sample, with manually appended dark spectrum bolded in black and the two endmembers (purest signal spectrum and purest background spectrum) selected by N-FINDR highlighted in orange and yellow. Center: plots of signal abundance maps with blue corresponding to a pixel with strong background spectrum and red corresponding to a pixel with strong signal spectrum. Right: extracted signal pixels that meet a thresholding requirement.

as on the position of the sample with respect to the sensor's aperture.

$$\vec{v'} = a \cdot \vec{v}_{sig} + b \cdot \vec{v}_{black} \quad (1)$$

In order to extract signal from background, a set of spectral endmember selection algorithms and unmixing algorithms are used [16]. Endmember selection and spectral unmixing are each important steps for processing multispectral data as they enable separation of an image into discrete regions. For instance, these algorithms are commonly used to distinguish between soil patches with high and low iron content in a spectral image taken by a drone or a satellite. The pixel deemed to represent the purest signature of a particular class is called an endmember.

In the current analysis, extremely low spatial resolution is obtained, with each pixel requiring an independent spectrum acquisition. However, only two endmembers are required for signal extraction: sample and background. The procedure is as follows: a spectrum was recorded of the velvet black background without any meteorite sample present. It is assumed to be a correct endmember selection and is manually appended to the end of each row of pixels. Three endmember selection algorithms were then applied to the dataset: the Purest Pixel Index (PPI) [17], Automatic Target Generation Process (ATGP) [18], and N-FINDR [19]. Each algorithm was set to identify two endmembers in each meteorite sample's dataset and was evaluated based on the number of samples in which the manually appended black endmember was selected (See Table 5). N-FINDR selected the black endmember in all cases, while the other two tested algorithms were weak in comparison. N-FINDR operates by computing the volume of a high-dimensional simplex formed by groups of pixels in spectral space. The group of pixels containing the endmembers will produce the highest-volume simplex.

Table 5: Endmember Algorithm Accuracy

Endmember Algorithm	Correct black endmember detection rate (%)
PPI	56.5%
ATGP	30.4%
N-FINDR	100%

Given the strong performance of N-FINDR in selecting the correct black endmember, the algorithm's selection for second endmember was used as the purest representation of signal. The results were then used in a

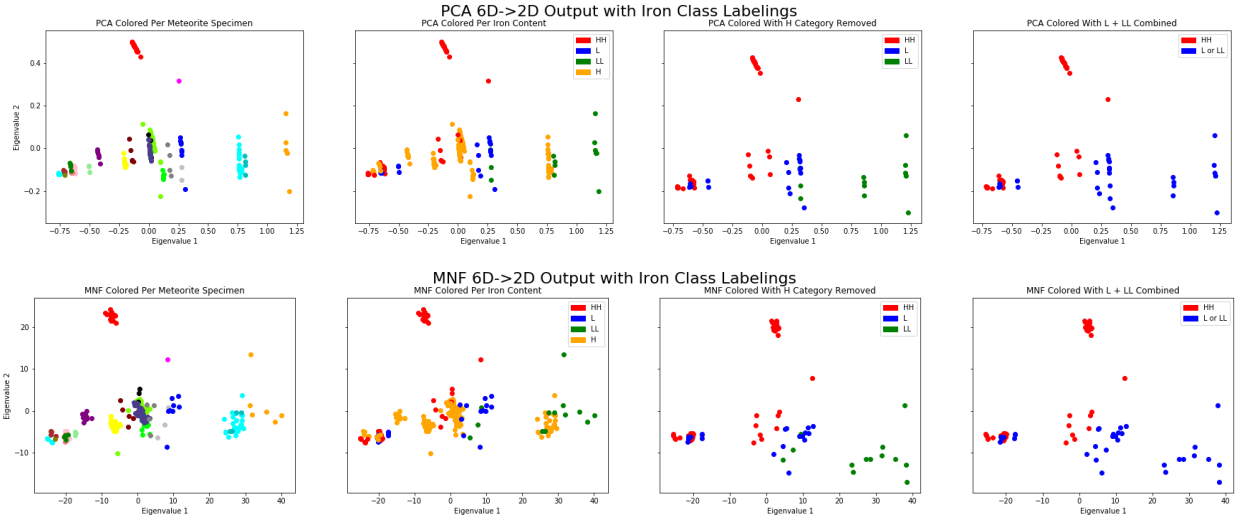

Figure 8: 6D-to-2D dimensionality reduction approaches (PCA, MNF) with results colored by iron content

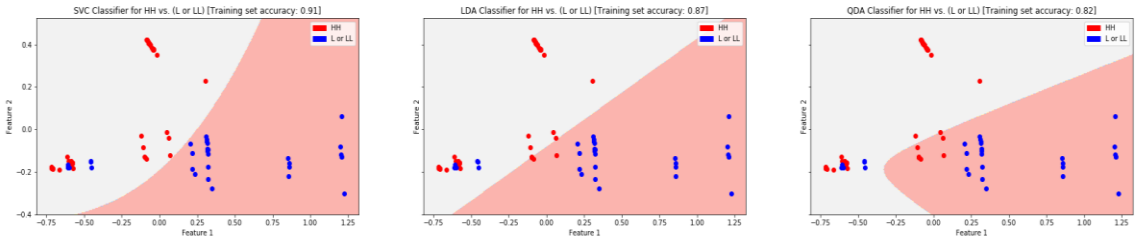

Figure 9: Visualization of three weighted classifiers trained on PCA 'HH' vs. 'L + LL' data. Training data prediction accuracy for the given classifiers are 91% (SVC) 87% (LDA) and 82% (QDA). The classifiers have yet to be verified with a test data set and thus overfitting is a risk.

least squares unmixing step with both the abundance nonnegative constraint (ANC) and the abundance sum-to-one constraint (ASC) applied.

The Least Squares algorithm determines the composition of each pixel in terms of the selected endmembers and is used to generate a per-pixel signal abundance map. Finally, two methods were compared for extracting a representative spectrum for each signal: a thresholding approach in which pixels deemed to be composed of sufficiently high signal percentage are kept (thresholds of 0.5, 0.75, and 0.85 used) and a decomposition method in which, of pixels composed of more than 75% signal, the appropriate percentage of background is subtracted out of the spectrum on the basis of Equation 1. In order to minimize the impact of artifacts added to the data from the ANC and ASC constraints, it was decided to proceed with a mid-level thresholding approach in wpectrhicsh spectra with 0.75 signal are kept and the remaining pixels are discarded.

The pre-processing steps as applied to two separate meteorite samples are shown in Figure 7.

Dimensionality Reduction

Once preprocessing is complete, analysis proceeds by reducing the dimensionality of the data to principal components that maximize variance in the data. Note that the dataset contains multiple pixels derived from each meteroite sample. Two methods are considered: standard principal component analysis (PCA) and a Minimum Noise Fraction algorithm (MNF) which is a modified PCA for spectral analysis in which a noise whitening step is first applied in order to remove correlation between spectral bands. When PCA is applied to the complete dataset, two principle components are found to explain 82.1% and 16.5% of the overall variance respectively; when PCA is run on the dataset with the 'H' chondrite class removed, two principal components explain 87.1% and 10.1% of the variance respectively.

Since the original dataset only contains 6 features, a set of artificial features were appended to the data that include ratios and squared ratios of all pairs of spectral band readings, as well as differences and squared differences between all pairs of spectral band readings. When PCA is run on the enlarged feature set for all data, two principal components explain 93.0% and 5.3% of the variance respectively; when PCA is run on the enlarged dataset with the 'H' chondrite class removed, two principal components explain 89.5% and 8.1% of the data respectively. In all cases, a visual examination of the reduced data shows that the most dominant trait for the dimension with largest variance is the meteoritic origin of the sample (a consequence of multiple pixels per sample considered in the analysis). Since this feature is irrespective of content in the sample and more a consequence of small dataset size, it may be of less importance for making iron content predictions. Therefore, since the second strongest eigenvector of the standard PCA analysis was found to explain greater percentage variance, standard PCA was used for remaining analysis.

Plots for the eigenvalues associated with each principle component are shown in Figure 8 with color corresponding to iron content. It is immediately clear upon visual inspection that the 'H' chondrite category will not be predictable using these axes. However, upon removing all 'H' samples from the dataset, a plausible separation between 'HH', 'L' and 'LL' samples is apparent. It is predominantly a result of the second strongest eigenvector's contribution. The separation is even more apparent when discriminating only between 'HH' vs. 'L or LL' – samples with highest (>90%) vs lowest (<25%) iron content.

Decision Boundaries

We seek to produce an decision boundary in low dimensional space that can be used to distinguish between high iron and low iron samples. To do so, a set of classifiers were trained to discriminate between the 'HH' and 'L or LL' classes using linear discriminant analysis (LDA), quadratic discriminant analysis (QDA) and support vector machine (SVM). In each case, spectra derived from the same meteorite sample are weighted such that each meteorite sample exerts equal influence on the classifier irrespective of how many pixels from the sample were preserved by the preprocessor.

Training data prediction accuracy for the given classifiers are 91% (SVC) 87% (LDA) 82% (QDA). The classifiers have yet to be validated with a test dataset and thus it is possible that the reported accuracy is a result of overfitting. Once the AS7263 is reporting spectra more predictably, the analysis will be rerun and a test dataset will be acquired and used for validation.

PROTOTYPE ROPE CRAWLING MECHANISM

Once the net has grappled onto the body of interest, a network of sensor nodes will crawl across the net's surface with an aim to collect high spatial resolution spectral data. A fully functional crawling mechanism will have the following mechanical design requirements: (1) firm grappling onto Kevlar rope's surface (2) precision rope crawling and location tracking (3) minimal slipping at variable rope angle (4) pointing control for sensor aperture and (5) (optional) two-axis crawling.

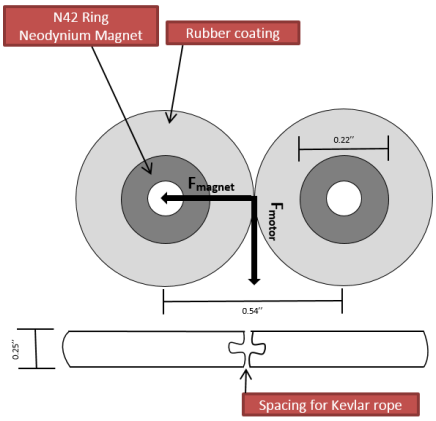

Figure 10: Magnetic Pinch Roller Design

Magnetic Pinch Roller Design

A first prototype was developed to address requirement (1) – the grappling approach. Inspired by techniques used in [13], a rubber coated magnetic pinch roller design is pictured in Figure 10.

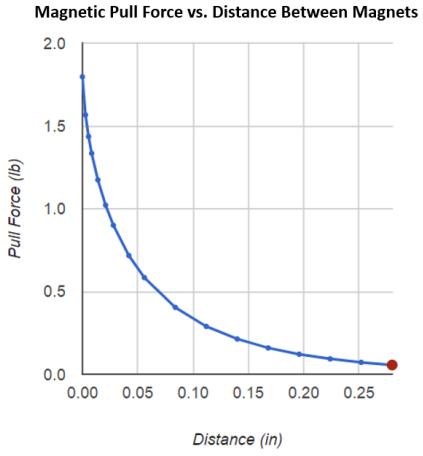

Figure 11: Calculated pull force WRT distance between magnets used to select rubber thickess

A relationship between magnet distance and resulting pull force is calculated and plotted in Figure 11. It is used to determine an appropriate rubber coating thickness to minimize motor torque requirements while preserving a sufficiently strong magnetic pinching effect. The selected design limits the magnetic pull force to 27.22g, corresponding to a separation of 0.54in between the two magnets. In order for the crawler's wheels to spin, the force applied by the motor must exceed the magnetic force between the rollers. The selected Pololu 136:1 Sub-Micro Plastic Gearmotor can tolerate an instantaneous torque of 550g·cm which easily suffices for the given setup.

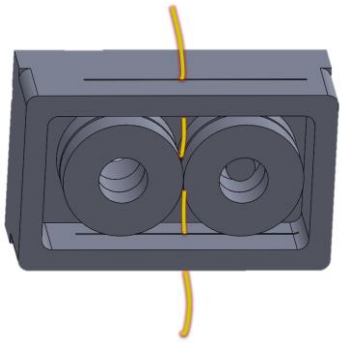

Figure 12: CAD rope crawling design

Prototype Manufacturing Approach

The manufacturing steps taken to produce the prototype are as follows: all key components were modeled in Solidworks (see Figure 12 for CAD). a 3D printed wheel with inlets sized for braided Kevlar rope was used to produce a silicone negative mold. This negative mold was subsequently used to construct flexible rubber wheels that were then placed over cylindrical neodymium magnets A ball bearing was press fit into a one of the magnetic wheel axels, and the motor shaft was press fit into the second magnetic wheel axel, in each case making use of supporting 3D printed parts. Finally, both the motor and ball bearing were press fit into a 3D-printed casing. The motor was powered via external power supply. The structure weighs 13.05g. Key steps of the process are pictured in Figure 13, and a video of initial crawling mechanism testing is available at https://vimeo.com/221468274. The resulting structure weighs 31.6g and the casing has dimensions of 1.5''x2''x 0.75''.

Evaluation

The pinch roller rope crawler design demonstrated the functionality of the basic rope climbing technique under consideration. For the second prototype, a thinner rubber will be tested as well both for weight savings and for increased magnetic pinching strength, despite the power requirement increase. Early thin rubber

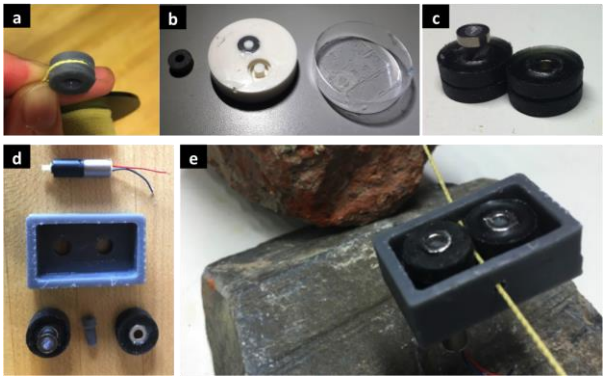

Figure 13 (a) 3D printed wheel with Kevlar rope in inlet (b) Molding process for creating rubber wheel (c) rubber wheels placed on cylindrical neodymium magnets, with ball bearing press fit onto left magnet (d) motor, casing, wheels (e) working prototype

prototypes were prone to ripping over a timescale of minutes after attachment to the magnetic cylinders. Therefore, tolerances will be adjusted to reduce the strain on the rubber. It may also be productive to test a spring-tensioned pinch rolling system in cases where the small body under study is likely to be magnetic.

The first prototype was very susceptible to rotation with respect to the Kevlar rope due to uneven weight distribution. This behavior is particularly important to address seeing as the spectral sensor may be acutely sensitive to incidence angle of light. A second prototype should more deliberately consider both the weight distribution of the overall bot as well as incorporate a mechanism for precision alignment of the sensor aperture with the imaging sample. Finally, the second prototype should consider adhesion methods for tensioning the rope and test the resilience of adhesion methods to the oscillations induced by robotic crawlers.

CONCLUSION + FUTURE WORK

We described a novel mission concept involving using a rope or a net as a mechanism to deploy a distributed sensor network across a low-gravity body of interest. We provide a broad list of possible application areas for the concept and hone in on an application in distributed spectral sensing. Some exploratory work towards building out a comprehensive mission concept is shared, including evaluation and preliminary analysis of a new-to-market spectroscope as well as a preliminary rope crawling mechanism. An analysis technique that may enable discrimination between high and low iron

content meteorite samples using six spectral band analysis technique is reviewed.

Immediate next steps ought to include creating a more robust optical setup to test the AS7263's halogen spectrum reading, developing a V2 crawling mechanism that addresses learnings from the first prototype, and commencing a study of net adhesion methods to be tested in micro-gravity conditions.

Alternative application areas to spectral sensing may also be considered prior to proceeding with mission development.

ACKNOWLEDGEMENTS

Thank you to Prof. Kerri Cahoy for project support, and to both the MIT Earth And Planetary Sciences department and to the Harvard Geological Museum for meteorite sample access.

References

1. Gärdsback, Mattias and Gunnar Tibert. "Deployment Control of Spinning Space Webs." *Journal of guidance, control, and dynamics* 32.1 (2009) 40-50
2. Sabatini, Marco, and Giovanni B. Palmerini. "Dynamics of a 3D rotating tethered formation flying facing the Earth." Aerospace Conference, 2007 IEEE. IEEE, 2007
3. Kaya, Nobuyuki, et al. "Crawling robots on large web in rocket experiment on Furoshiki deployment." *Journal of the British Interplanetary Society* 58. 11-12 (2005): 403-406
4. Nakasuka, Shinichi, et al. "Large Membrane "Furoshiki Satellite" applied to phased array antenna and its sounding rocket experiment." *Acta Astronautica* 58.8 (2006): 395-400
5. Summerer, Leopold, et al. "Robots Moving on a Loose Net in Microgravity – Results from the Japanese Furoshiki Sounding Rocket Experiment." *9th ESA workshop on advanced space technologies for robotics and automation (ASTRA), ESTEC, Noordwijk, The Netherlands.* 2006.
6. Sinn, Thomas, et al. "Results of REXUS12's Suaineadh Experiment: Deployment of a spinning space web in microgravity conditions." *63rd International Astronautical Congress.* 2012.
7. Tsuda, Yuichi, et al. "Achievement of IKAROS – Japanese deep space solar sail demonstration mission." *Acta Astronautica* 82.2 (2013): 183-1888
8. McKenzie, D., et al. "Space webs: final report." *ESA, Advanced Concepts Team, Rept 5* (2006).
9. Yang, Leping, et al. "Dynamics and Design of Space Nets for Orbital Capture." Springer. (2017).
10. Guang, Zhai, and Zhang, Jing-rui. "Space tether net system for debris capture and removal." *Intelligent 4th International Conference on Human-Machine Systems and Cybernetic (IHMSC), 2012.* Vol. 1. IEEE, 2012
11. Hang, Panfeng, et al. "Dynamics and configuration control of the maneuvering-net space robot system." *Advances in Space Research* 55.4 (2015): 1004-1014
12. Rutkin, Aviva Hope. "Magnetic net to snare space debris set to launch." (2014): 19
13. Dementyev, Artem, et al. "Rovables: Miniature on Body Robots as Mobile Wearables." *Proceedings of the 29th Annual Symposium on User Interface Software and Technology.* ACM, 2016.
14. http://ams.com/eng/Products/Spectral-Sensing/Multi-spectral-Sensing/AS7263
15. Johnson, Jeffrey R., et al. "Constraints on iron sulfate and iron oxide mineralogy from ChemCam visible/near-infrared reflectance spectroscopy of Mt. Sharp basal units, Gale Crater, Mars" *American Mineralogist* 101.7 (2016): 1501-1514
16. http://pysptools.sourceforge.net/
17. Chang, Chein I., and Antonio, Plaza." A fast iterative algorithm for implementation of pixel purity index." *IEEE Geoscience and Remote Sensing Letters* 3.1 (2006): 63-67.
18. A. Plaza, C.-I. Chang, "Impact of Initialization on Design of Endmember Extraction Algorithms", Geoscience and Remote Sensing, IEEE Transactions on, vol. 44, no. 11, pgs. 3397-3407, 2006.
19. Winter, Michael E. "N-FINDR: An algorithm for fast autonomous spectral end-member determination in hyperspectral data." *SPIE's International Symposium on Optical Science, Engineering, and Instrumentation. International Society for Optics and Photonics, 1999.*